# Kinetics of the Gas-Phase Reaction of OH with Chlorobenzene

**Mikhail G. Bryukov,[†] Vadim D. Knyazev,*[,‡] William M. Gehling, Jr.,[†] and Barry Dellinger*[,†]**

*Department of Chemistry, Louisiana State University, Baton Rouge, Louisiana 70803, and Research Center for Chemical Kinetics, Department of Chemistry, The Catholic University of America, Washington, DC 20064*

*Received: May 26, 2009; Revised Manuscript Received: July 20, 2009*

The kinetics of the reaction of hydroxyl radicals with chlorobenzene was studied experimentally using a pulsed laser photolysis/pulsed laser induced fluorescence technique over a wide range of temperatures, 298−670 K, and at pressures between 13.33 and 39.92 kPa. The bimolecular rate constants demonstrate different behavior at low and high temperatures. At room temperature, $T = 298.8 \pm 1.5$ K, the rate constant is equal to $(6.02 \pm 0.34) \times 10^{-13}$ cm$^3$ molecule$^{-1}$ s$^{-1}$; at high temperatures (474−670 K), the rate constant values are significantly lower and have a positive temperature dependence that can be described by an Arrhenius expression $k_1(T) = (1.01 \pm 0.35) \times 10^{-11} \exp[(-2490 \pm 170\ \text{K})/T]$ cm$^3$ molecule$^{-1}$ s$^{-1}$. This behavior is consistent with the low-temperature reaction being dominated by reversible addition and the high-temperature reaction representing abstraction and addition−elimination channels. The potential energy surface of the reaction was studied using quantum chemical methods, and a transition state theory model was developed for all reaction channels. The temperature dependences of the high-temperature rate constants obtained in calculations using the method of isodesmic reactions for transition states (IRTS) and the CBS-QB3 method are in very good agreement with experiment, with deviations smaller than the estimated experimental uncertainties. The G3//B3LYP-based calculated rate constants are in disagreement with the experimental values. The IRTS-based model was used to provide modified Arrhenius expressions for the temperature dependences of the rate constant for the abstraction and addition−elimination (Cl replacement) channels of the reaction.

## I. Introduction

Understanding the reactions of chlorinated hydrocarbons is an essential component of efficient incineration of hazardous wastes, assessing the environmental effects of open burning of wastes, and developing methods for production of chlorine-containing commoditites. Reaction kinetic modeling of these processes is important to optimizing their efficiency and developing tools to otherwise minimize their impacts on human health and welfare. However, success of such modeling is limited by the lack of fundamental information on the rates and products of a large number of elementary reactions involving chlorinated hydrocarbon species.[1]

The hydroxyl radical plays a key role in the chemistry of combustion processes, with initial attacks by OH on closed-shell species serving as a source of a large variety of reactive radical intermediates. In this work, we report the results of our experimental and computational study of the gas-phase reaction of the hydroxyl radical with chlorobenzene

$$\text{OH} + \text{C}_6\text{H}_5\text{Cl} \rightarrow \text{products} \qquad (1)$$

Reaction 1 has previously been studied experimentally.[2−5] The only earlier direct determination of the rate constant, that of Wallington et al.,[3] focused on the low-temperature range, where addition to the benzene ring is the dominant process. The maximum experimental temperature was 438 K, where the reverse of the addition reaction became dominant, and the abstraction and substitution channels just began to become important. However, only two data points (at 363 and 438 K) were determined at temperatures where reverse reaction was important. The observed absence of a positive temperature dependence suggests that the experimental temperatures were not sufficiently high for the reversible addition reaction to become unimportant compared to the abstraction and displacement channels. The only study at higher temperature where the addition is completely reversed is that of Mulder and Louw.[4] These authors used a relative rates technique to determine the ratio of the rate constant of reaction 1 to that of the reaction of OH with benzene at one temperature, 563 K.

The current experimental study of the kinetics of reaction 1 has been performed over a wide temperature range from 298 K (to compare with the earlier low-temperature studies) to 670 K. The temperature dependence of the rate constant was determined under the high-temperature conditions where the reaction is dominated by H abstraction and Cl displacement channels that are more relevant to combustion conditions. The kinetics and mechanism of reaction 1 were studied computationally, with the results providing recommendations for the temperature dependences of the rate constants of these channels over wide temperature ranges.

## II. Experimental Section

**II.1. Experimental Technique.** Absolute rate coefficients for the reaction of hydroxyl radicals with chlorobenzene were measured using the pulsed laser photolysis/pulsed laser induced fluorescence (PLP/PLIF) technique. All experiments were carried out in a slow-flow, heatable quartz reactor (reaction cell) under pseudo-first-order conditions with a large excess of chlorobenzene. A detailed description of the experimental setup, data acquisition methodology, and data

* Corresponding authors. Experimental part: BarryD@LSU.edu (B.D). Theoretical part: knyazev@cua.edu (V.D.K.).
[†] Louisiana State University.
[‡] The Catholic University of America.

10.1021/jp9049186 CCC: $40.75 
Published on Web 09/03/2009

processing has been given in our previous articles.[6,7] Therefore, only the details necessary to understand the present measurements are considered here.

Hydroxyl radicals were generated by the 351 nm (XeF excimer) pulsed laser photolysis (the repetition frequency was 10 Hz) dissociation of HONO molecules[8,9]

$$\mathrm{HONO} + h\upsilon(351\ \mathrm{nm}) \rightarrow \mathrm{OH} + \mathrm{NO} \qquad (2)$$

This method of OH generation was applied to eliminate the possible effects of the laser photolysis excitation and dissociation of chlorobenzene on the observed OH decay rates (vide infra).

After the excimer laser pulse, a second pulse at approximately 282 nm from a Nd:YAG-pumped, frequency-doubled, tunable pulsed dye laser induced excitation of the hydroxyl radicals via the $A^2\Sigma^+ - X^2\Pi$ (1−0) transition. Hydroxyl radicals were observed via fluorescence from the (1−1) and (0−0) bands at 308−316 nm.[9,10] The fluorescent radiation emitted perpendicular to the plane defined by the two laser beams was detected with a photomultiplier tube, using appropriate filters (308 nm peak transmission) to minimize the contribution of scattered light. The signal from the photomultiplier was amplified and then recorded by a digital oscilloscope. The oscilloscope obtained the integrated voltage averaged for a desired number of accumulated signals (typically 100−200) at a given time delay between the excimer laser and Nd:YAG laser pulses. This time delay was varied to record kinetic information using a digital delay generator. The value, $S_t$, received from the integration of the average voltage signal is a sum of two components: the integral from the average LIF signal of OH radicals, $S_{OH}$, which is proportional to the absolute OH concentration, and the integral from the average scattered light signal, $S_{sc}$. $S_{sc}$ was directly measured in the absence of the hydroxyl radicals in the reactor.

We used four individually controlled flows of $N_2$ or He (main carrier gas flow), $H_2O$/ $N_2$ or He, HONO/ $N_2$ or He, and $C_6H_5Cl$/ $N_2$ or He to prepare a reaction gas mixture. $H_2O$ was transported to the reaction cell by bubbling a flow of $N_2$ or He through water at controlled pressure and temperature in a thermostabilized saturator. HONO was made from the dropwise addition of a 0.2 M aqueous solution of $NaNO_2$ to a 20% sulfuric acid aqueous solution in a flask or a saturator which were kept in an ice bath (at a temperature near 0 °C). The small flow of $N_2$ or He through the flask or the saturator was varied to control the HONO concentration entering the reaction cell. These mixtures were replaced daily.[8] Chlorobenzene was accurately, manometrically diluted with nitrogen or helium using a Pyrex vacuum system. To minimize systematic error in chlorobenzene concentration determinations, mixtures of $C_6H_5Cl$ in $N_2$ or He were prepared with different concentrations of chlorobenzene in the range 0.72−0.98%. All flows were premixed using a delivery system and then directed through the reaction cell. The total flow rate ranged between 5.8 and 9.6 STP $cm^3\ s^{-1}$. The total pressure in the reactor was measured with the 100.00 or 1000.0 Torr (1 Torr = 133.322 Pa) capacitance manometers. The reaction gas temperature in the detection zone was monitored with a retractable chromel−alumel thermocouple. The maximum total uncertainty in the measurements of the reaction temperatures, $T$, did not exceed 0.5% of $T$. [6,7]

The molecular concentration of chlorobenzene in the detection zone was calculated by means of multiplying the three values: the total concentration derived from the measured total pressure and temperature using the ideal gas law, the molecular partial concentration in the flow carrying chlorobenzene, and the value from the ratio of the flow carrying chlorobenzene to the total gas flow rate.

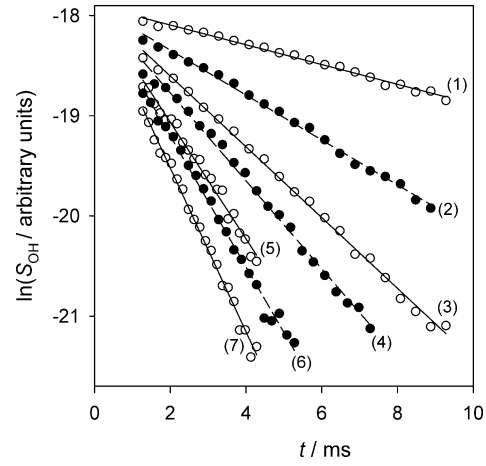


**Figure 1.** Examples of relative OH concentration temporal profiles obtained under the following experimental conditions: nitrogen buffer gas; temperature $T = 665$ K; total pressure $P = 26.72$ kPa (200.4 Torr); $[H_2O] = 1.1 \times 10^{16}$ molecules $cm^{-3}$; $[HONO] \approx 10^{13}$ molecules $cm^{-3}$; $[C_6H_5Cl] = 0.0$, $5.73 \times 10^{14}$, $8.91 \times 10^{14}$, $1.36 \times 10^{15}$, $1.95 \times 10^{15}$, $2.38 \times 10^{15}$, and $2.92 \times 10^{15}$ molecules $cm^{-3}$ for profiles 1−7, respectively.

The chemicals utilized in this work had the following specified minimum purities (and were supplied by): $N_2$, 99.999% (Capitol Welders Supply Co.); He, 99.999% (Capitol Welders Supply Co.); $H_2O$, ACS reagent grade (Sigma-Aldrich); $H_2SO_4$, 95−98% aqueous solution, ACS reagent grade (Sigma-Aldrich); $NaNO_2$, 99.5%, super free-flowing (Sigma-Aldrich); $C_6H_5Cl$, 99.99%, CHROMASOLV$^R$, for HPLC (Sigma-Aldrich). Chlorobenzene was purified by vacuum distillations prior to use. The chemical purity of this sample was examined by GC/MS (Agilent Technologies 6890N Gas Chromatography System/5973 Mass Selective Detector). After purification by vacuum distillation, the purity of the sample of chlorobenzene exceeded the specifications provided by Sigma-Aldrich and was at least 99.996%. The GC/MS analysis revealed the presence of benzene in the sample of chlorobenzene as the main impurity at a level less than 0.0036% and only trace levels of other impurities. These small concentrations had a negligible effect on the observed OH decay rates.

**II.2. Reaction Rate Measurements and Data Processing.** All experiments measuring the bimolecular rate coefficients for the reaction of OH with $C_6H_5Cl$ were performed under pseudo-first-order kinetics conditions with a large excess of chlorobenzene with respect to the initial concentration of the hydroxyl radical, $[OH]_0$, ranging approximately from $8 \times 10^{10}$ to $7 \times 10^{11}$ molecules $cm^{-3}$ in the detection zone. The initial concentrations of OH radicals were estimated in a way similar to that previously described.[8] Accurate knowledge of the initial OH radical concentration is not needed to determine the bimolecular rate coefficients because all experiments were performed under pseudo-first-order conditions with a large excess of chlorobenzene. The estimated OH radical detection limit, defined by unity signal-to-noise ratio at 150 accumulated signals, was found to range from $1 \times 10^8$ to $6 \times 10^8$ molecules $cm^{-3}$ depending on the experimental conditions.

A typical set of relative OH concentration temporal profiles (a set of experiments) are depicted in Figure 1 as a plot of $\ln(S_{OH}) = \ln(S_t - S_{sc})$ versus time delays, $t$. Water vapor

was always added to the reaction mixtures at concentrations that were varied from $1.5 \times 10^{15}$ to $1.4 \times 10^{16}$ molecules $cm^{-3}$ from set to set of experiments. This was done to ensure that the rotational and vibrational equilibration of OH radicals to the Boltzmann distribution proceeded sufficiently fast to have a negligible effect on the measured rate coefficients.[11] Furthermore, over the entire experimental temperature range, temporal profiles of the formation of OH($X^2\Pi$, $v = 0$) under typical experimental conditions in the absence of chlorobenzene were also obtained. Prompt OH($X^2\Pi$, $v = 0$) formation was observed that was always much faster (at least 4 times) than the initial detection time delays, $t_0$, in all relative OH concentration decays used in the rate constant determinations. This indicates that the rotational and vibrational equilibration of OH radicals to the Boltzmann distribution proceeded fast enough to be neglected at the time delays $t \geq t_0$ that would have otherwise led to nonprompt OH($X^2\Pi$, $v = 0$) formation.

Each set of experiments was analyzed assuming pseudo-first-order kinetics behavior of the hydroxyl radical decay to determine bimolecular rate coefficients of the OH + $C_6H_5Cl$ reaction:

$$\ln(S_{OH}) = \ln(S_t - S_{SC}) = \text{constant} - k't \qquad \text{(I)}$$

where the effective first-order rate coefficient, $k'$, is given by

$$k' = k_1[C_6H_5Cl] + k_0 \qquad \text{(II)}$$

Here, $k_1$ is the bimolecular rate coefficient of the reaction OH + $C_6H_5Cl$, $[C_6H_5Cl]$ is the molecular concentration of chlorobenzene, and $k_0$ is the effective first-order rate coefficient of the hydroxyl radical decay due to OH reaction with HONO, possible OH reactions with background impurities in the buffer gas, $H_2O$, and HONO, and OH diffusion and flow out of the detection zone (OH background loss). The effective first-order rate coefficient values, $k'$, were derived from linear least-squares fits of the experimental values $\ln(S_{OH})$ to eq I. These least-squares fits and all next least-squares fits in the present work were performed with no weighting of the data points.

Examples of effective first-order rate coefficient dependencies on molecular chlorobenzene concentration are presented in Figure 2. We determined the bimolecular rate coefficient, $k_1$, from the slope of the least-squares straight line drawn through the $k'$ versus $[C_6H_5Cl]$ data points including the (0, $k_0$) point, where $k_0$ was derived from the OH temporal profile directly measured at zero concentration of the molecular substrate.

**II.3. Experimental Results.** The kinetics study of the gas-phase OH radical reaction with $C_6H_5Cl$ was performed over the temperature range 298−670 K and at pressures between 13.33 and 39.92 kPa. The conditions and results of the experiments used to determine the values of the absolute bimolecular rate coefficients for reaction 1 are compiled in Table 1.

The initial concentration of hydroxyl radicals was varied from experimental set to set by changing the photolysis laser intensity or the concentration of HONO over wide ranges: 26−64 mJ $pulse^{-1}$ $cm^{-2}$ and $10^{13}$−$6 \times 10^{13}$ molecules $cm^{-3}$, respectively. The measured rate coefficients demonstrate no correlation with pressure and initial concentration of OH radicals within the experimental ranges. The fact that the rate coefficients are independent of the initial OH radical concentration indicates the absence of any influence from potential secondary reactions on the kinetics of OH radical decay due to the low values of

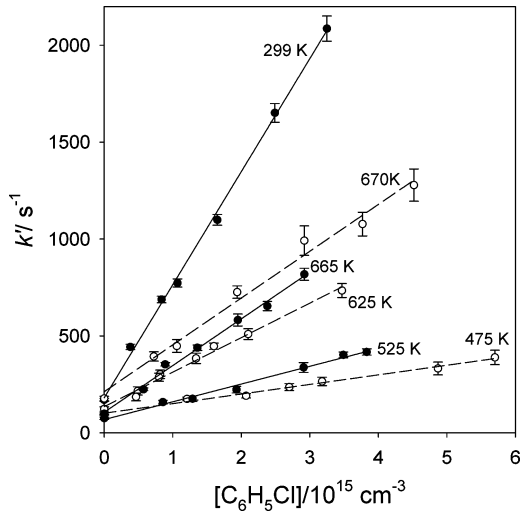


**Figure 2.** Examples of experimentally obtained $k'$ versus $[C_6H_5Cl]$ dependences.

$[OH]_0$ in the detection zone ($[OH]_0 \approx (8-70) \times 10^{10}$ molecules $cm^{-3}$). There was no correlation between the measured rate coefficients and the photolysis laser intensity within the experimental range. This fact allows one to consider the possible effects of the reaction between OH and the products of laser photolysis of $C_6H_5Cl$ on the rate coefficient measurements as negligible in our experiments. At the highest temperatures in this study, the absence of any potential influence from thermal decomposition of chlorobenzene and HONO on the final results was verified by measuring the bimolecular rate coefficients at different bulk flow velocities and reaction pressures that varied by factors of 1.3 and 1.5, respectively.

We could not measure the absolute bimolecular rate coefficient for the reaction of OH with $C_6H_5Cl$ in the temperature range ~350−450 K because nonexponential OH decays were observed under these experimental conditions. Similar behavior was observed in previous works[3,12] for the OH reactions with benzene and halogenated benzene. The explanation is as follows. At room temperature and lower, the addition channels probably dominate the reaction of hydroxyl radical with chlorobenzene, resulting in the formation of three different $C_6H_5ClOH$ isomers as the main products. These radicals are stabilized by buffer gas and do not decompose at the time of detection. At temperatures between ~350 and 450 K, decomposition of $C_6H_5ClOH$ becomes important on the time scale of the experiments and relaxation to equilibrium in the reversible addition process results in nonexponential OH decay profiles. At temperatures above ~450 K and pressures above ~100 Torr of nitrogen, the addition channels are completely reversed and thus provide practically no contribution to OH decay.

In the temperature range 474−670 K, the kinetics of the OH decays followed the pseudo-first-order law and the derived bimolecular rate coefficients from our experimental data did not correlate with reaction pressure. The bimolecular rate coefficients for the OH + $C_6H_5Cl$ reaction determined in our study are plotted along with those from the earlier studies[2−4] in Figure 3. The $k_1(T)$ rate coefficient data set for reaction 1 exhibits a positive temperature dependence in the temperature range 474−670 K. The linear least-squares fit of this data set to the

**TABLE 1: Conditions and Results of Experiments on the Reaction of Hydroxyl Radicals with Chlorobenzene**

| no.[a] | *T*/K | *P*/kPa | $[C_6H_5Cl]$ range/ $10^{14}$ molecules cm$^{-3}$ | $I^b$/ mJ pulse$^{-1}$ cm$^{-2}$ | $[OH]_0$/ $10^{10}$ molecules cm$^{-3}$ | $k_1{}^c$/ $10^{-14}$ cm$^3$ molecule$^{-1}$ s$^{-1}$ |
|---|---|---|---|---|---|---|
| 1 | 298 | 13.37 | 3.56−30.6 | 37 | 70 | 61.5 ± 5.4 |
| 2* | 299 | 13.42 | 3.81−32.5 | 56 | 40 | 58.3 ± 2.3 |
| 3* | 299 | 13.38 | 3.79−30.1 | 54 | 35 | 60.9 ± 3.5 |
| 4* | 299 | 13.42 | 3.77−30.2 | 23 | 10 | 61.7 ± 2.8 |
| 5* | 299 | 13.38 | 3.76−34.8 | 22 | 10 | 58.4 ± 2.9 |
| 6 | 474 | 13.35 | 12.1−48.7 | 64 | 25 | 4.95 ± 0.43 |
| 7 | 505 | 26.72 | 8.92−54.4 | 37 | 30 | 7.38 ± 0.54 |
| 8 | 525 | 13.33 | 8.57−38.3 | 61 | 40 | 9.16 ± 0.81 |
| 9 | 545 | 26.64 | 7.21−38.3 | 34 | 20 | 11.3 ± 0.8 |
| 10 | 585 | 26.72 | 5.9−41.6 | 30 | 9 | 14.7 ± 1.2 |
| 11 | 625 | 26.74 | 4.64−34.7 | 37 | 15 | 17.8 ± 1.4 |
| 12 | 665 | 26.72 | 5.63−29.8 | 26 | 8 | 24.1 ± 1.7 |
| 13 | 670 | 39.92 | 7.27−45.2 | 26 | 15 | 24.2 ± 2.4 |

[a] Experiment number. Helium was used as the main carrier gas in experiments marked with asterisks, and nitrogen was used as the main carrier gas in unmarked experiments. [b] Photolysis laser intensity. OH was produced by the PLP of HONO at 351 nm in all experiments. [c] Error limits represent $2\sigma$ statistical uncertainties only. The maximum estimated systematic uncertainty is 5% of the bimolecular rate coefficient value (see refs 6 and 7 for details).

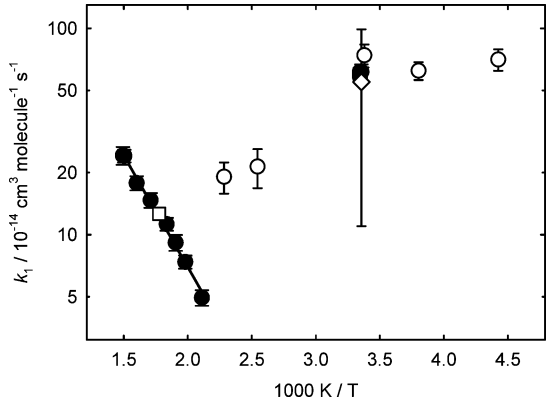


**Figure 3.** Temperature dependence of the bimolecular rate coefficient for the reaction of OH with $C_6H_5Cl$ displayed in Arrhenius coordinates. The symbols represent the experimental data from several groups: filled circles, results of the current study; open circles, Wallington et al.;[3] open diamond with very large uncertainly limits, Edney et al.;[2] open square, Mulder and Louw[4] (relative rate value converted in this work using the reference reaction rate data from Tully et al.[12]). The black solid line represents the Arrhenius fit of eq III.

Arrhenius expression yields the following expression for the bimolecular rate constant temperature dependence:

$$k_1(T) = (1.01 \pm 0.35) \times 10^{-11} \times \exp[(-2490 \pm 170\ \text{K})/T]\ \text{cm}^3\ \text{molecule}^{-1}\ \text{s}^{-1} \quad (474-670\ \text{K}) \quad \text{(III)}$$

This Arrhenius expression reproduces the experimental data very well, with the maximum and average square deviations being only 7.5 and 4.4%, respectively.

### III. Potential Energy Surface and Transition State Theory Model of the OH + $C_6H_5Cl$ Reaction

**III.1. Potential Energy Surface.** The potential energy surface (PES) of reaction 1 was studied using quantum chemical approaches. The density functional BH&HLYP[13,14] method with the aug-cc-pVDZ basis set[15] was used for the optimization of molecular structures and calculation of vibrational frequencies. The version of the BH&HLYP functional implemented in Gaussian 03[16] was used, which, as described in the Gaussian manual, is different from that reported in the literature.[13] Energies of the transition states relative to the reactants were calculated using the IRTS method[17,18] (isodesmic reactions for transition states) using the prototype reactions

$$OH + C_6H_6 \rightarrow H_2O + C_6H_5 \quad (3a)$$

and

$$OH + C_6H_6 \rightarrow C_6H_6OH \quad (3b)$$

as the reference reactions. BH&HLYP/aug-cc-pVDZ-level energy values were used for the IRTS calculations.

In addition, two composite high-level single-point energy methods were used for the calculation of energy barriers and enthalpies of reactions: CBS-QB3[19,20] and G3//B3LYP.[21] All PES calculations lead to the same qualitative conclusions regarding the mechanism of reaction 1; energy values quoted in the text henceforth are those obtained in the IRTS calculations for transition states and in CBS-QB3 calculations for stable species. These energies include vibrational zero-point energies unless stated otherwise. The results of the PES study are summarized in Table 2 and Figure 4, and the detailed information is given in the Supporting Information (Table 1S). The Gaussian 03 program[16] was used in all potential energy surface (PES) calculations.

The mechanism of reaction 1 is qualitatively similar to that of reactions 3a and 3b (refs 22 and 23 and references cited therein). The pathways leading to $C_6H_4Cl + H_2O$ products are those of H atom abstraction:

$$OH + C_6H_5Cl \rightarrow H_2O + 2\text{-}C_6H_4Cl \quad (1a)$$

$$OH + C_6H_5Cl \rightarrow H_2O + 3\text{-}C_6H_4Cl \quad (1b)$$

$$OH + C_6H_5Cl \rightarrow H_2O + 4\text{-}C_6H_4Cl \quad (1c)$$

Addition of OH to the ring leads to the formation of several isomers of the $C_6H_5ClOH$ adduct:

$$OH + C_6H_5Cl \rightarrow 2\text{-}C_6H_5ClOH \quad (1d)$$

$$OH + C_6H_5Cl \rightarrow 3\text{-}C_6H_5ClOH \quad (1e)$$

$$OH + C_6H_5Cl \rightarrow 4\text{-}C_6H_5ClOH \quad (1f)$$

Reaction 1, like that of OH with benzene, is dominated by addition at low temperatures. Addition is reversed at temperatures above ~400 K, and high-temperature reaction is that of H-abstraction. An important difference from the OH + $C_6H_6$ reaction is that addition of OH to the ring in the α position to chlorine results in substitution:

**TABLE 2: Energies of Reactants, Products, and Stationary Points on the PES of Reaction 1 Obtained in Quantum Chemical Calculations[a]**

| | method | | | |
|---|---|---|---|---|
| species[b] | BH&HLYP[c] | IRTS[d] | CBS-QB3 | G3//B3LYP |
| $OH\cdots C_6H_5Cl$ | −5.73 | | | |
| $1\text{-}C_6H_5ClOH$ | −73.82 | | | |
| $2\text{-}C_6H_5ClOH$ | −53.77 | | −79.87 | −70.79 |
| $3\text{-}C_6H_5ClOH$ | −51.56 | | −74.70 | |
| $4\text{-}C_6H_5ClOH$ | −54.85 | | −79.82 | −71.52 |
| $C_6H_5OH\cdots Cl$ | −94.25 | | −97.47 | −88.49 |
| $Cl + C_6H_5OH$[e] | −57.95 | | −52.29 | −56.52 |
| $H_2O + 2\text{-}C_6H_4Cl$ | 5.01 | | −7.61 | −6.15 |
| $H_2O + 3\text{-}C_6H_4Cl$ | −1.39 | | −14.93 | −13.20 |
| $H_2O + 4\text{-}C_6H_4Cl$ | 0.91 | | −12.32 | −10.39 |
| TS(1a) | 41.84 | 21.01 | 20.40 | 25.85 |
| TS(1b) | 38.08 | 17.26 | 18.40 | 21.72 |
| TS(1c) | 38.61 | 17.79 | 18.61 | 22.30 |
| TS(1d) | 23.01 | 2.66 | 2.59 | 12.05 |
| TS(1e) | 24.00 | 3.66 | 4.58 | 14.93 |
| TS(1f) | 21.14 | 0.79 | 2.23 | 12.39 |
| TS(1 g) | 39.32 | 18.97 | 14.09 | 24.03 |
| TS(1g-2)[f] | 74.04 | | | |

[a] Energy values are given in kJ $mol^{-1}$ relative to OH + $C_6H_5Cl$ and include zero-point vibrational energy (ZPE). [b] See text for the description of the individual PES stationary points. [c] With the aug-cc-pVDZ basis set. [d] Isodesmic reactions for transition states. [e] The experimental value is −64.8 ± 1.8 kJ $mol^{-1}$.[37−39] [f] The transition state between $1\text{-}C_6H_5ClOH$ and $C_6H_5OH\cdots Cl$ (exists at the BH&HLYP/aug-cc-pVDZ level but was not found using the B3LYP/CBSB7 and B3LYP/6-31G(d) methods used in CBS-QB3 and G3//B3LYP calcuations; see text).

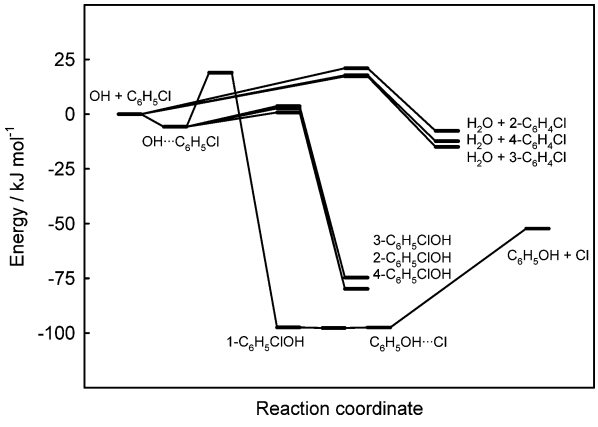


**Figure 4.** Potential energy surface of reaction 1. Energies of transition states are those obtained in IRTS calculations. Energies of stable species were obtained using the CBS-QB3 method.

$$OH + C_6H_5Cl \rightarrow (1\text{-}C_6H_5ClOH) \rightarrow C_6H_5OH\cdots Cl \rightarrow Cl + C_6H_5OH \quad (1g)$$

The unstable adduct $1\text{-}C_6H_5ClOH$, presented in parentheses in the equation of reaction 1g, has a very low barrier for transformation to the $C_6H_5OH\cdots Cl$ complex (the BH&HLYP-aug-cc-pVDZ level of calculations yields a barrier of 0.4 kJ $mol^{-1}$ without ZPE and −0.2 with ZPE). This adduct does not exist as a PES minimum if the B3LYP method is used for structure optimization with smaller basis sets, such as CBSB7 and 6-31G(d) used in the CBS-QB3 and G3//B3LYP methods, as confirmed by relaxed C−Cl distance scans. For the $C_6H_5OH\cdots Cl$ complex, the large energy difference (~76 kJ $mol^{-1}$) between the "entrance" and the "exit" transition states makes stabilization highly unlikely. Thus, channel 1g is considered as a substitution channel with the reaction bottleneck located at the PES saddle point for OH addition to the ring.

The reaction paths of channels (1d−1g) proceed through a shallow van der Waals minimum (weakly bound $OH\cdots C_6H_5Cl$ complex) on the reactant side, followed by addition energy barriers. The structure of the $OH\cdots C_6H_5Cl$ complex is similar to that found for the OH + $C_6H_6$ reaction, [22] with OH oriented perpendicular to the benzene ring and the H atom of the hydroxyl radical oriented toward the ring. Application of the IRTS method to the reaction of addition of OH to benzene ring is somewhat problematic because the barrier for addition, if any, is very low. Application of transition state theory for such reactions generally requires the use of variational formalism, which, in turn, requires the knowledge of the potential energy surface over an extended range of reaction coordinates. Nevertheless, an attempt was made to use the IRTS technique for the addition reaction channels 1d−1f and the addition−elimination channel 1g using the prototype reaction 3b as the reference reaction. The energy barrier value for the reference reaction of 1.13 kJ $mol^{-1}$ was obtained in fitting the calculated rate constants to the experimental data of Tully et al.[12] at 250 and 298 K, which are in agreement with the results of other direct determinations [3,24,25] of the rate constant of reaction 3a in this temperature range and thus were taken as representative of these data. The resultant values of the addition energy barriers for channels 1d−1f resulting in the formation of adducts are low and similar in values, ranging from 0.8 to 3.7 kJ $mol^{-1}$. The addition barrier for the reaction channel 1g is significantly higher, 14.1 kJ $mol^{-1}$.

The abstraction energy barriers (channels 1a−1c) are higher than those of addition and range from 17.3 to 21.0 kJ $mol^{-1}$. Following the approach of Seta et al.,[23] the PES of anharmonic bending motions in these transition states (in-plane and out-of-plane C−H−O angles in the C···H···OH structure) were scanned with all other geometric parameters fixed at the optimized values. The obtained potential energy profiles were used in transition state theory calculations of the rate constants (see below).

The IRTS formalism[17,18] requires knowledge of a rate constant of a reference reaction, in which the chemical transformation taking place and the structure of the transition state are similar to those of the reaction being studied. For example, a reference reaction for the abstraction channels 1a−1c should have a transition state with the C···H···OH structure; i.e., it should be another reaction of abstraction of a hydrogen atom by the OH radical. Reaction 3a was consequently selected as the reference reaction for channels 1a−1c. The rate constant of this reaction has been determined as a function of temperature in

the 621−1709 K temperature range,[12,23,26] with good agreement between the results of three groups. The PES of reaction 3a was studied using the BH&HLYP/aug-cc-pVDZ method−basis set combination. The rate constants for the reference reaction were calculated using transition state theory, and the energy barrier was adjusted to reproduce the experimental $k_{3a}(T)$ temperature dependence (see below for the details of the transition state theory calculations). The resultant energy barrier is $E_{3a} = 14.73$ kJ mol$^{-1}$. The energy barriers for reaction channels 1a−1c were obtained by adding to $E_{3a}$ the 0 K enthalpy $\Delta H$(ISO) of the isodesmic reactions

$$C_6H_5Cl + C_6H_5\cdots H\cdots OH^{\ddagger} = C_6H_6 + x\text{-}C_6H_4Cl\cdots H\cdots OH^{\ddagger} + \Delta H(\mathrm{ISO}) \quad (4)$$

where $x = 2-4$. The resultant values of the energy barriers are presented in Table 2 and Figure 4.

**III.2. Rate Constant Calculations.** The rate constants of reaction channels 1a−1g were calculated using transition state theory. [27] A tunneling correction was included for the abstraction channels (1a−1c) using the Eckart formula[28] within the barrier-width method.[29−31] The values of the barrier width parameter were obtained in fitting the energy profiles in the vicinity of the PES saddle points obtained by following the intrinsic reaction coordinate[32,33] with the Eckart function.[28] Properties of the reactants, products, and transition states were obtained in quantum chemical calculations performed at the BH &HLYP/aug-cc-pVDZ level, except for OH and $H_2O$, for which experimental properties were used. The energy barriers were determined in IRTS, CBS-QB3, or G3//B3LYP calculations, as described above.

In transition state theory calculations, partition functions of all species involved were obtained using the approximation of harmonic oscillators and free or hindered rotors, except for the two significantly nonharmonic degrees of freedom in the abstraction transition states. These degrees of freedom correspond to bending of the C···H···OH structures. Calculation of the partition functions of these bending modes was performed using the method of Seta et al.[23] Potential energy and reduced moments of inertia were obtained as functions of the wagging and rocking angles, and the energy levels were calculated by numeric solution of the Schrödinger equation using the FGH1D program.[34] Reduced moments of inertia for these degrees of freedom as well as for torsional motions were calculated using the formulas of Pitzer and Gwinn;[35,36] partition functions of torsions were calculated using the Pitzer−Gwinn approximation.[35]

In the IRTS method, the energy barriers for the reference reactions (3a and 3b) were fitted to reproduce the experimental[12,23,26] rate constant data. The resultant calculated temperature dependences of the rate constants are compared with the experimental values in Figure 1S in the Supporting Information.

The calculated rate constant temperature dependences are compared with the experimental rate constants in Figure 5, where $k(T)$ plots for individual channels of reaction 1, as well as that of the overall reaction, are presented. As can be seen from the plot, the model reproduces the experimental $k_1(T)$ dependence very well over the 474−670 K temperature range. The average deviation from the experiment is 6%, lower than the 8% average statistical uncertainty of the experimental values and comparable to the estimated 5% systematic uncertainty of the experiment (Table 1). The agreement at room temperature is somewhat poorer, with the calculated $k_1(298\ \mathrm{K}) = 4.65 \times 10^{-13}$ cm$^3$ molecule$^{-1}$ s$^{-1}$, 23% lower than the average experimental value of $(6.02 \pm 0.34) \times 10^{-13}$ cm$^3$ molecule$^{-1}$ s$^{-1}$. Calculated rate constant values at individual temperatures are given in the Supporting Information (Table 2S).

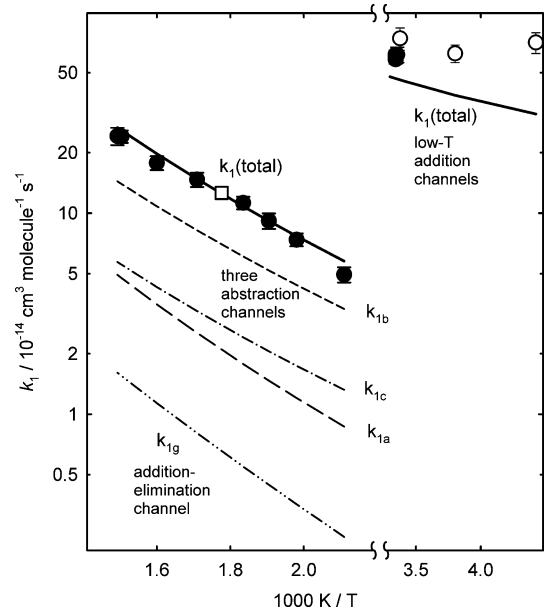


**Figure 5.** Comparison of the experimental and calculated temperature dependences of the rate constants of reaction 1. Symbols: experimental values of the current study (filled black circles), Wallington et al.[3] (open circles, low temperatures), Mulder and Louw[4] (open square). Lines: reaction models of the current study obtained in IRTS calculations. Heavy lines represent the overall rate constant (sum of channels), and thin lines represent individual channels in the high-temperature region.

Use of the CBS-QB3 energies for the transition states also results in very good agreement with the experiment at high temperature (average deviation is also less than the experimental uncertainty). The room temperature CBS-QB3-based calculated rate constant is $3.54 \times 10^{-13}$ cm$^3$ molecule$^{-1}$ s$^{-1}$ which is 41% lower than the experimental value. The rate constants for individual abstraction channels obtained using the CBS-QB3 energies agree with the IRTS values within 25% over the experimental temperature range. However, the larger value for the barrier of the addition−elimination channel 1g obtained using the CBS-QB3 method results in a more significant difference in the rate constants: the IRTS and CBS-QB3 values of $k_{1g}(T)$ differ by factors of 2.4−3.5 over the same temperature range. G3//B3LYP energy barriers are higher than those obtained in IRTS and CBS-QB3 calculations, with larger differences obtained for the addition and addition elimination channels. As a result, the G3//B3LYP-based rate constants are lower than the experimental values by a factor of 2 in the high-temperature range and by 2 orders of magnitude at room temperature. The temperature dependences of the rate constants calculated using the CBS-QB3 and G3//B3LYP energies are presented in Tables 3S and 4S and Figures 2S and 3S in the Supporting Information.

Rate constants for the abstraction (1a−1c) and addition−elimination (1g) channels were calculated using the IRTS energies over wide ranges of temperatures. The resultant $k(T)$ dependences can be represented with the following modified Arrhenius expressions:

$$k_{1a} = 1.69 \times 10^{-20} T^{2.64} \times \exp(-1513\ \mathrm{K}/T)\ \mathrm{cm}^3\ \mathrm{molecule}^{-1}\ \mathrm{s}^{-1} \quad (500-3000\ \mathrm{K}) \quad (\mathrm{IV})$$

$$k_{1a} = 3.64 \times 10^{-31} T^{6.01} \times \exp(+320\ \mathrm{K}/T)\ \mathrm{cm^3\ molecule^{-1}\ s^{-1}} \quad (200-600\ \mathrm{K}) \quad (V)$$

$$k_{1b} = 3.39 \times 10^{-20} T^{2.59} \times \exp(-1046\ \mathrm{K}/T)\ \mathrm{cm^3\ molecule^{-1}\ s^{-1}} \quad (500-3000\ \mathrm{K}) \quad (VI)$$

$$k_{1b} = 5.17 \times 10^{-27} T^{4.74} \times \exp(+140\ \mathrm{K}/T)\ \mathrm{cm^3\ molecule^{-1}\ s^{-1}} \quad (200-600\ \mathrm{K}) \quad (VII)$$

$$k_{1c} = 1.89 \times 10^{-20} T^{2.54} \times \exp(-1080\ \mathrm{K}/T)\ \mathrm{cm^3\ molecule^{-1}\ s^{-1}} \quad (500-3000\ \mathrm{K}) \quad (VIII)$$

$$k_{1c} = 1.10 \times 10^{-27} T^{4.83} \times \exp(+177\ \mathrm{K}/T)\ \mathrm{cm^3\ molecule^{-1}\ s^{-1}} \quad (200-600\ \mathrm{K}) \quad (IX)$$

$$k_{1g} = 3.09 \times 10^{-19} T^{2.10} \times \exp(-1867\ \mathrm{K}/T)\ \mathrm{cm^3\ molecule^{-1}\ s^{-1}} \quad (200-3000\ \mathrm{K}) \quad (X)$$

Since the differences between the overall calculated rate constants and the experimental values are well within the uncertainties of the experiments, eqs IV−X can be used for the purpose of extrapolation of the experimental results to temperatures outside the experimental range.

## IV. Discussion

The current study provides the first determination of the rate constant of reaction 1 as a function of temperature in the high-temperature range, where the addition channels (1d−1f) are reversed and the overall reaction is dominated by the abstraction (1a−1c) and substitution (addition−elimination, 1g) channels. Rate constants were obtained in direct experiments over the 474−670 K range. In addition, the room-temperature rate constant (primarily addition) was determined. The results are in agreement with earlier studies where such comparison can be made (Figure 3). The room-temperature rate constant determined in the current work coincides with the directly obtained values of Wallington et al.[3] and the relative-rates result of Edney et al.[2] The high-temperature results are in very good agreement with the relative-rate single temperature (563 K) determination of Mulder and Louw.[4] The study of Wallington et al.[3] covered the temperature range 226−438 K; three of the five data points were obtained at low temperatures and two data points are at 363 and 438 K. The two higher-temperature rate constant values are approximately a factor of 3 lower than those at the low temperatures, indicating that addition is mostly reversed. However, it seems likely that the addition channels and the corresponding reverse reactions regenerating OH through the decomposition of the adducts still influenced the kinetics of OH decay because the reported rate constant values indicate either absence of temperature dependence or a slightly negative dependence. These values are also approximately an order of magnitude higher than extrapolation of our high-temperature Arrhenius dependence to lower temperatures would suggest (Figure 3).

Comparison of the results of the computational study results of reaction 1 with the experimental results demonstrated a very good agreement between the calculated and experimental rate constants in the high-temperature region, with the differences being less than the uncertainties of the experimental values (Figure 5). The observed agreement serves as an additional confirmation of the high accuracy of the IRTS method.[17,18] At the same time, the agreement at room temperatures is poorer, with 23% difference between the experimental and calculated rate constant values. Also, the calculated low-temperature rate constants have a weak positive temperature dependence while the experimental results of Wallington et al. in the 226−296 K range suggest absence of temperature dependence within the data scatter. As was mentioned above, application of the IRTS method to the addition reaction channels is expected to be problematic because of the very low, if any, barrier for addition. Thus, poorer agreement with the experiment is not surprising. At the same time, it is worth mentioning that the 23% disagreement at room temperature corresponds to a 0.65 kJ $\mathrm{mol^{-1}}$ error in the energy barrier, which is rather small for a computation-based method.

Use of the CBS-QB3 energy barriers also results in very good agreement between the calculated and experimental high-temperature rate constants. The resultant $k(T)$ dependence differs very little from the IRTS-based one and thus is not presented in Figure 5 to avoid plot congestion; instead, CBS-QB3 rate constants are presented in a graph and a table in the Supporting Information (Figure 2S and Table 2S). The rate constants for the individual reaction channels 1a−1c obtained in CBS-QB3-based calculations (with BH&HLYP/aug-cc-pVDZ vibrational frequencies) differ from those obtained in IRTS calculations by only 6, 22, and 17%, respectively, over the experimental temperature range. The difference between the rate constants for the addition−elimination channel 1g obtained in the CBS-QB3-based and IRTS calculations is significantly larger: a factor of 2.9, on average, over the same temperature range, reflecting the 4.9 kJ $\mathrm{mol^{-1}}$ difference in the energy barrier values between these two methods.

One unfortunate consequence of the imperfect agreement of the IRTS-based calculated rate constant at room temperature with experiment is the unknown uncertainty of the energy barrier for the reaction channel 1g, that of addition−elimination, or substitution of Cl in chlorobenzene for OH. The barrier of 1.13 kJ $\mathrm{mol^{-1}}$ was derived for the reference reaction 3b within the IRTS method from the analysis of the low-temperature addition rate constant data.[12] The low value indicates that variational transition state theory is more appropriate for modeling this addition reaction. However, the barrier for reaction 1g is relatively large (19 kJ $\mathrm{mol^{-1}}$), which means that the location of the dynamic saddle point on the PES is fixed and variational effects in application of transition state theory, if any, can be expected to be much smaller than in the case of the reference reaction. This difference in the degree of variational effects between the reference reaction and the reaction being studied can be expected to result in the uncertainty in the IRST energy barrier for reaction channel 1g that is larger than the above value of 0.65 kJ $\mathrm{mol^{-1}}$ derived from the analysis of the room-temperature rate constant values. On the basis of these considerations, we can recommend an estimated uncertainty of +3/−7 kJ $\mathrm{mol^{-1}}$ for the energy barrier of the reaction channel 1g (the average coincides with the difference between the CBS-QB3 and IRTS values). When used with eq X for the rate constant, this energy barrier uncertainty translates into the uncertainties in the rate constants equal to factors of 17/3.4 at 298 K, 5.4/2.1 at 500 K, 2.3/1.4 at 1000 K, 1.5/1.2 at 2000 K, and 1.3/1.1 at 3000 K (the first number refers to the factor for increasing the rate constant value and the second to that for decreasing it). Alternatively, one can choose to use the CBS-QB3-based temperature dependence of the channel 1g rate constant

$$k_{1g}(\mathrm{CBS\text{-}QB3}) = 3.09 \times 10^{-19} T^{2.10} \times \exp(-1279\ \mathrm{K}/T)\ \mathrm{cm^3\ molecule^{-1}\ s^{-1}} \quad (200-3000\ \mathrm{K}) \quad (XI)$$

with the +8/−2 kJ $\mathrm{mol^{-1}}$ uncertainty in the activation energy.

**Acknowledgment.** This research was partially supported by NIEHS grant RO1ES015450 and the LSU Patrick F. Taylor Chair. The authors would like to thank Dr. J. N. Crowley, Dr. S. M. Lomnicki, and Dr. V. L. Orkin for helpful discussions and advice.

**Supporting Information Available:** Results of the quantum chemical calculations on the potential energy surfaces and rate constant calculations for reactions 1 and 3 (Tables 1S−4S, Figures 1S−3S, 25 pages). This material is available free of charge via the Internet at http://pubs.acs.org.

## References and Notes

(1) Tsang, W. *Combust. Sci. Technol.* **1990**, *74*, 99.
(2) Edney, E. O.; Kleindienst, T. E.; Corse, E. W. *Int. J. Chem. Kinet.* **1986**, *18*, 1355.
(3) Wallington, T. J.; Neuman, D. M.; Kurylo, M. J. *Int. J. Chem. Kinet.* **1987**, *19*, 725.
(4) Mulder, P.; Louw, R. *J. Chem. Soc., Perkin Trans. 2* **1987**, 1167.
(5) Mulder, P.; Louw, R. *Int. J. Chem. Kinet.* **1988**, *20*, 577.
(6) Bryukov, M. G.; Dellinger, B.; Knyazev, V. D. *J. Phys. Chem. A* **2006**, *110*, 936.
(7) Bryukov, M. G.; Knyazev, V. D.; Lomnicki, S. M.; McFerrin, C. A.; Dellinger, B. *J. Phys. Chem. A* **2004**, *108*, 10464.
(8) Gilles, M. K.; Burkholder, J. B.; Gierczak, T.; Marshall, P.; Ravishankara, A. R. *J. Phys. Chem. A* **2002**, *106*, 5358.
(9) Wollenhaupt, M.; Carl, S. A.; Horowitz, A.; Crowley, J. N. *J. Phys. Chem. A* **2000**, *104*, 2695.
(10) D'Ottone, L.; Campuzano-Jost, P.; Bauer, D.; Hynes, A. J. *J. Phys. Chem. A* **2001**, *105*, 10538.
(11) Silvente, E.; Richter, R. C.; Hynes, A. J. *J. Chem. Soc., Faraday Trans.* **1997**, *93*, 2821.
(12) Tully, F. P.; Ravishankara, A. R.; Thompson, R. L.; Nicovich, J. M.; Shah, R. C.; Kreutter, N. M.; Wine, P. H. *J. Phys. Chem.* **1981**, *85*, 2262.
(13) Becke, A. D. *J. Chem. Phys.* **1993**, *98*, 1372.
(14) Lee, C. T.; Yang, W. T.; Parr, R. G. *Phys. Rev. B* **1988**, *37*, 785.
(15) Kendall, R. A.; Dunning, T. H., Jr.; Harrison, R. J. *J. Chem. Phys.* **1992**, *96*, 6796.
(16) Frisch, M. J.; Trucks, G. W.; Schlegel, H. B.; Scuseria, G. E.; Robb, M. A.; Cheeseman, J. R.; Montgomery, J. A., Jr.; Vreven, T.; Kudin, K. N.; Burant, J. C.; Millam, J. M.; Iyengar, S. S.; Tomasi, J.; Barone, V.; Mennucci, B.; Cossi, M.; Scalmani, G.; Rega, N.; Petersson, G. A.; Nakatsuji, H.; Hada, M.; Ehara, M.; Toyota, K.; Fukuda, R.; Hasegawa, J.; Ishida, M.; Nakajima, T.; Honda, Y.; Kitao, O.; Nakai, H.; Klene, M.; Li, X.; Knox, J. E.; Hratchian, H. P.; Cross, J. B.; Bakken, V.; Adamo, C.; Jaramillo, J.; Gomperts, R.; Stratmann, R. E.; Yazyev, O.; Austin, A. J.; Cammi, R.; Pomelli, C.; Ochterski, J. W.; Ayala, P. Y.; Morokuma, K.; Voth, G. A.; Salvador, P.; Dannenberg, J. J.; Zakrzewski, V. G.; Dapprich, S.; Daniels, A. D.; Strain, M. C.; Farkas, O.; Malick, D. K.; Rabuck, A. D.; Raghavachari, K.; Foresman, J. B.; Ortiz, J. V.; Cui, Q.; Baboul, A. G.; Clifford, S.; Cioslowski, J.; Stefanov, B. B.; Liu, G.; Liashenko, A.; Piskorz, P.; Komaromi, I.; Martin, R. L.; Fox, D. J.; Keith, T.; Al-Laham, M. A.; Peng, C. Y.; Nanayakkara, A.; Challacombe, M.; Gill, P. M. W.; Johnson, B.; Chen, W.; Wong, M. W.; Gonzalez, C.; Pople, J. A. *Gaussian 03*, revision C.02; Gaussian, Inc.: Wallingford, CT, 2004.
(17) Knyazev, V. D. *J. Phys. Chem. A* **2002**, *106*, 11603.
(18) Knyazev, V. D. *J. Phys. Chem. A* **2003**, *107*, 11082.
(19) Montgomery, J. A., Jr.; Frisch, M. J.; Ochterski, W.; Petersson, G. A. *J. Chem. Phys.* **1999**, *110*, 2822.
(20) Montgomery, J. A., Jr.; Frisch, M. J.; Ochterski, W.; Petersson, G. A. *J. Chem. Phys.* **2000**, *112*, 6532.
(21) Baboul, A. G.; Curtiss, L. A.; Redfern, P. C.; Raghavachari, K. *J. Chem. Phys.* **1999**, *110*, 7650.
(22) Chen, C. C.; Bozzelli, J. W.; Farrell, J. T. *J. Phys. Chem A* **2004**, *108*, 4632.
(23) Seta, T.; Nakajima, M.; Miyoshi, A. *J. Phys. Chem A* **2006**, *110*, 5081.
(24) Lorenz, K.; Zellner, R. *Ber. Bunsen-Ges. Phys. Chem.* **1983**, *87*, 629.
(25) Witte, F.; Urbanik, E.; Zetzsch, C. *J. Phys. Chem.* **1986**, *90*, 3251.
(26) Madronich, S.; Felder, W. *J. Phys. Chem.* **1985**, *89*, 3556.
(27) Johnston, H. S. *Gas Phase Reaction Rate Theory*; The Ronald Press: New York, 1966.
(28) Eckart, C. *Phys. Rev.* **1930**, *35*, 1303.
(29) Knyazev, V. D.; Bencsura, A.; Stoliarov, S. I.; Slagle, I. R. *J. Phys. Chem.* **1996**, *100*, 11346.
(30) Knyazev, V. D.; Slagle, I. R. *J. Phys. Chem.* **1996**, *100*, 16899.
(31) Bryukov, M. G.; Slagle, I. R.; Knyazev, V. D. *J. Phys. Chem. A* **2001**, *105*, 3107.
(32) Fukui, K. *Acc. Chem. Res.* **1981**, *14*, 363.
(33) Gonzalez, C.; Schlegel, H. B. *J. Phys. Chem.* **1990**, *94*, 5523.
(34) Johnson, R. D. I. *FGH1D*, PC/Windows program for computing vibrational levels for non-harmonic potentials; National Institute of Standards and Technology: Gaithersburg, MD.
(35) Pitzer, K. S.; Gwinn, W. D. *J. Chem. Phys.* **1942**, *10*, 428.
(36) Pitzer, K. S. *J. Chem. Phys.* **1946**, *14*, 239.
(37) Chase, M. W., Jr. *J. Phys. Chem. Ref. Data* **1998**, *9* (Monograph), 1.
(38) Cox, J. D. *Pure Appl. Chem.* **1961**, *2*, 125–128.
(39) Platonov, V. A.; Simulin, Yu. N. *Russ. J. Phys. Chem.* **1985**, *59*, 179.

JP9049186